# The effect of rocking stapes motions on the cochlear fluid flow and on the basilar membrane motion

Edom, E ; Obrist, D ; Henniger, R ; Kleiser, L ; Sim, J H ; Huber, A M

Abstract: The basilar membrane (BM) and perilymph motion in the cochlea due to rocking stapes motion (RSM) and piston-like stapes motion (PSM) is modeled by numerical simulations. The full Navier-Stokes equations are solved in a two-dimensional box geometry. The BM motion is modeled by independent oscillators using an immersed boundary technique. The traveling waves generated by both stimulation modes are studied. A comparison of the peak amplitudes of the BM motion is presented and their dependence on the frequency and on the model geometry (stapes position and cochlear channel height) is investigated. It is found that the peak amplitudes for the RSM are lower and decrease as frequency decreases whereas those for the PSM increase as frequency decreases. This scaling behavior can be explained by the different mechanisms that excite the membrane oscillation. Stimulation with both modes at the same time leads to either a slight increase or a slight decrease of the peak amplitudes compared to the pure PSM, depending on the phase shift between the two modes. While the BM motion is dominated by the PSM mode under normal conditions, the RSM may lead to hearing if no PSM is present or possible, e.g., due to round window atresia.

DOI: https://doi.org/10.1121/1.4824159

# The effect of rocking stapes motions on the cochlear fluid flow and on the basilar membrane motion

Elisabeth Edom,[a] Dominik Obrist, Rolf Henniger, and Leonhard Kleiser
*Institute of Fluid Dynamics, ETH Zurich, Sonneggstrasse 3, 8092 Zurich, Switzerland*

Jae Hoon Sim and Alexander M. Huber
*Department of Otorhinolaryngology, Head and Neck Surgery, University Hospital of Zurich, Frauenklinikstrasse 36, 8091 Zurich, Switzerland*

(Received 3 December 2012; revised 5 September 2013; accepted 17 September 2013)

The basilar membrane (BM) and perilymph motion in the cochlea due to rocking stapes motion (RSM) and piston-like stapes motion (PSM) is modeled by numerical simulations. The full Navier–Stokes equations are solved in a two-dimensional box geometry. The BM motion is modeled by independent oscillators using an immersed boundary technique. The traveling waves generated by both stimulation modes are studied. A comparison of the peak amplitudes of the BM motion is presented and their dependence on the frequency and on the model geometry (stapes position and cochlear channel height) is investigated. It is found that the peak amplitudes for the RSM are lower and decrease as frequency decreases whereas those for the PSM increase as frequency decreases. This scaling behavior can be explained by the different mechanisms that excite the membrane oscillation. Stimulation with both modes at the same time leads to either a slight increase or a slight decrease of the peak amplitudes compared to the pure PSM, depending on the phase shift between the two modes. While the BM motion is dominated by the PSM mode under normal conditions, the RSM may lead to hearing if no PSM is present or possible, e.g., due to round window atresia.
 [http://dx.doi.org/10.1121/1.4824159]

PACS number(s): 43.64.Kc, 43.64.Bt [KG] Pages: 3749–3758

## I. INTRODUCTION

The cochlea is the mammalian hearing organ. Vibrations of the stapes of the middle ear lead to movements of the fluid in the cochlear ducts and generate a traveling wave on the BM. Motions of this membrane stimulate sensory receptor cells in the organ of Corti which leads to the perception of sound.

The investigation of the motion pattern of the stapes extends from the works of Stuhlman (1937) and Békésy (1960) to more recent studies, e.g., Hato *et al*. (2003) and Sim *et al*. (2010). For all considered species, both translational ("piston-like") and rotational ("rocking," "tilting") motion components are reported: Especially for stimulations at frequencies above 1 kHz (Hato *et al*., 2003) the stapes moves not only perpendicularly to its footplate but also rotates around the long and short axes of the footplate.

The influence of such rocking stapes movements (RSM) on the sense of hearing is an open issue. The piston-like motion of the stapes (PSM) generates a net fluid flow and pressure differences in the cochlea. These excite the basilar membrane (BM) and hence lead to the perception of sound. Because purely RSM components push the same fluid volume out of the cochlea as into it, the production of any net fluid flow and of pressure differences across the BM due to these motion components is doubted. Therefore, any possible contribution of RSM to the hearing is put in question by several authors (Decraemer *et al*., 2007; Voss *et al*., 1996).

Nevertheless, there is experimental evidence that cochlear activity is generated by RSM: from their measurements of compound action potentials in guinea pigs for controlled stapes motion, Huber *et al*. (2008) and Eiber *et al*. (2012) reported that neuronal activities due to rocking components of the stapes motion were clearly observed.

In several studies, possible effects of the fluid motion originating from RSM have been discussed: Decraemer *et al*. (2007) suspected that the RSM "must cause the fluid to slosh back and forth in a small volume behind the footplate" and that this local fluid motion would not excite any pressure wave which can propagate further into the cochlea. Hato *et al*. (2003) examined the three-dimensional motion of the stapes footplate in human temporal bones and concluded that the RSM generates no net fluid shift but a local fluid flow in a region close to the footplate of which it is unknown whether it affects hearing. In a study on the numerical modeling of cochlear hydrodynamics, Pozrikidis (2008) computed the response due to a dipole source at the oval window. This model for the RSM led to peak amplitudes of the BM which were significantly smaller than those induced by the PSM (modeled as a monopole source).

In the present work, we compare the BM motion and the fluid flow generated by PSM and RSM by means of numerical simulations. We consider a box geometry instead of the actual complex geometry of the cochlea. Velocity amplitudes at the oval window (OW) are chosen, first, constant for all frequencies and, second, corresponding to constant sound pressure level in the ear canal for all frequencies. We present and compare the flow fields evoked by RSM and by PSM. A detailed analysis of the BM peak amplitudes and their

[a]Author to whom correspondence should be addressed. Electronic mail: edom@ifd.mavt.ethz.ch

dependence on the inflow velocity, on the stimulation frequency and on the stapes position is given. We document the BM motion generated by PSM and RSM separately and by the combined motion for different phase shifts.

It will be shown that both RSM and PSM evoke traveling waves on the BM. These waves show almost no qualitative differences except that the peak amplitudes are higher for the PSM. The difference amounts to 10 dB and more, increasing as frequency decreases. The peak amplitudes for the RSM will be shown to decrease as frequency decreases whereas they increase as frequency decreases for the PSM. The scaling behavior of the BM peak amplitudes for RSM will be investigated in detail and it will be shown that the BM excitation is generated by different mechanisms for the respective stimulation modes. The numerical results together with related clinical studies indicate that the BM is stimulated even if only rotational stimulation of the cochlea is permitted, e.g., due to pathological conditions. Under normal conditions with mixed cochlea stimulation, the BM displacement is dominated by the PSM. The RSM leads to rather small changes which either increase or decrease the amplitudes depending on the phase difference between the two stimulation modes.

## II. GOVERNING EQUATIONS AND MODELING

### A. Governing equations

The lymphatic fluid within the cochlea is mechanically similar to water (Steele *et al.*, 1995). The lymphatic flow can be considered incompressible because the acoustic wave length is significantly larger than the length of the cochlea. Only at the highest physiological frequencies, compressibility effects might become relevant (Lighthill, 1981). Such effects will not be considered here.

Therefore, the dynamics of the lymph are well described by the Navier–Stokes equations for an incompressible flow,

$$\nabla \cdot \boldsymbol{u} = 0, \tag{1}$$

$$\mathrm{Str}\frac{\partial \boldsymbol{u}}{\partial t} + (\boldsymbol{u}\cdot\nabla)\boldsymbol{u} = -\nabla p + \frac{1}{\mathrm{Re}}\nabla^2\boldsymbol{u} + \boldsymbol{q} \tag{2}$$

(Drazin and Riley, 2006), which are given here in dimensionless form, where $\boldsymbol{u}$ denotes the velocity vector, $t$ the time, $p$ the pressure, and $\boldsymbol{q}$ the vector of field forces which will be used to introduce the effect of the BM on the flow. The Strouhal number

$$\mathrm{Str} = f^*\frac{L^*}{U^*} \tag{3}$$

is a dimensionless frequency where the dimensional frequency $f^*$ has been used to render the time dimensionless. The variable Re represents the Reynolds number, given by

$$\mathrm{Re} = \frac{U^*L^*}{\nu^*}, \tag{4}$$

with the maximum velocity $U^*$ of the stapes motion, the length $L^*$ of the stapes footplate, and the kinematic viscosity $\nu^*$. The superscript * denotes a dimensional quantity. Although the Reynolds number for the cochlear flow turns out to be less than unity (see Sec. III for the reference values) we use the full Navier–Stokes equations instead of the linear unsteady Stokes equations to ensure that we also account for weak nonlinear flow phenomena (Lighthill, 1992). However, the results presented in this work are not affected noticeably by the nonlinear term of the Navier–Stokes equations, i.e., they would remain unaltered if the unsteady Stokes equations were solved.

At the walls, no-slip boundary conditions are imposed, i.e., zero velocity at the bounding walls, and inflow/outflow velocities at the positions of the oval and round windows. These velocities are prescribed normal to the rest positions of the windows. It can be shown by a Taylor expansion that this approximation for the round and the oval window motion is accurate to the order of $x_s^2$, where $x_s$ denotes the displacement of the stapes perpendicular to the footplate. This displacement is small with respect to the characteristic length $L^*$ such that usage of the inflow/outflow conditions is justified.

The stapes velocity oscillates sinusoidally in time with frequency $f^*$ between the normalized maximum and minimum velocity $\pm 1$.

The BM motion is modeled by the motion of an array of independent oscillators along the BM which are governed by

$$m\frac{\partial^2\eta}{\partial t^2} + r\frac{\partial\eta}{\partial t} + k\eta = \Delta p, \tag{5}$$

where $\eta$ denotes the transversal displacement of the membrane, $m$, $r$, and $k$ its mechanical properties mass, linear damping coefficient, and stiffness, respectively, and $\Delta p$ the pressure difference across the membrane. A similar approach has already been used in previous works, e.g., Peterson and Bogert (1950) and Lesser and Berkley (1972).

The inertia of the fluid moved by the BM dominates the inertia of the BM itself. An effect of the mass $m$ on the BM motion can only be noticed for exceedingly high mass values. Therefore, we choose $m = 0$. This is in accordance with findings by de la Rochefoucauld and Olson (2007) for low to moderately high frequencies.

Furthermore, we neglect the structural damping within the BM ($r = 0$), because it is assumed that the major energy dissipation takes place in the boundary layers of the BM and at the cochlear walls. These boundary layers are fully resolved in our model such that the fluid viscosity provides the damping to the system.

Values for the graded stiffness $k$ are given in Sec. III.

### B. Computational modeling

The Navier–Stokes equations (2) are solved in a two-dimensional rectangular box. The oval window (OW) is positioned parallel to the BM on top of the scala vestibuli (SV), the round window (RW) orthogonal to the BM on the front side of the scala tympani (ST), cf. Fig. 1. On these sections of the boundaries, inflow/outflow is prescribed (Sec. II A). The modes of the stapes motion, PSM and RSM, are indicated in Fig. 1 by arrows [see also Fig. 11(a)].

The Navier–Stokes equations are discretized with a third-order explicit Runge–Kutta integration scheme in time

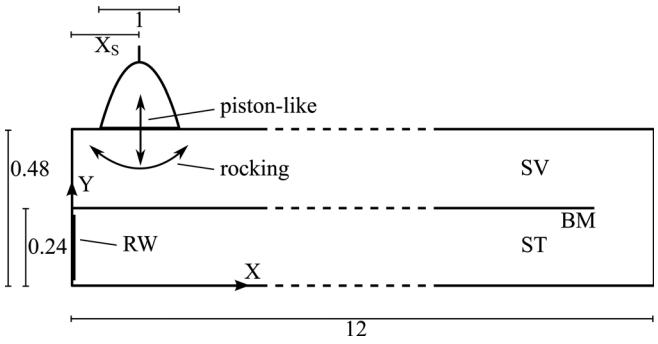


FIG. 1. Sketch of the computational domain.

and with sixth-order finite-differences in space. We used staggered Cartesian grids for the velocity and pressure fields. The utilized code is optimized for a massively parallel computation of very large flow problems and was thoroughly validated for different fluid dynamical applications (Henniger *et al.*, 2010).

The computational grid is stretched such that the mesh width $\Delta Y$ becomes smaller towards the walls and the BM. Its resolution is frequency-dependent in order to resolve the boundary layers and ranges from $100 \times 3000$ to $320 \times 9200$ points. The smallest mesh width at the position of the BM ranges from $4 \times 10^{-4}$ to $2 \times 10^{-3}$ (relative to $L^*$), depending on the stimulation frequency.

The fluid-structure interaction of the perilymph and the BM is modeled by a variant of the immersed boundary method by Peskin (2002). The immersed boundary method has already been applied in the field of cochlear mechanics by Beyer (1992) and Givelberg and Bunn (2003). In this method, the BM acts on the fluid through the field force $\boldsymbol{q}$ in Eq. (2). In the mobility formulation used here (Fig. 2), the BM is modeled as a one-dimensional manifold which is represented by discrete material points that are moving with the fluid. The number of points for the BM corresponds to the number of axial grid points. The deflected material points lead to a pressure difference $\Delta p$ according to Eq. (5) which is transformed into a field force $\boldsymbol{q}$ on the surrounding grid points of the fluid.

We interpolate the fluid velocities with a bilinear scheme to determine the velocity at the material points of the BM. The forces acting on the fluid are distributed bilinearly onto the velocity grids. The temporal integration scheme of the membrane motion is the same as for the fluid flow. The BM is the only immersed boundary and there are no rigid immersed boundaries, contrarily to the models by Beyer (1992) and Givelberg and Bunn (2003). The bounding walls of the cochlea are implemented as rigid walls via homogeneous Dirichlet boundary conditions for the velocities. These boundary conditions are satisfied when solving the pressure Poisson equation and the momentum equation for the flow velocities in an iterative manner (SIMPLE algorithm; Ferziger and Perić, 2002).

The spatial membrane computation is first-order accurate due to the velocity interpolation. This limits the overall convergence rate. Nevertheless, tests have shown that the numerical "leakage" through the BM (due to interpolation errors) remains below 0.1% with respect to the fluid volume moved by the stapes. Increasing the spatial resolution reduces this leakage even further.

The simulations were carried out on a personal computer with Intel i7-2600 cores (3.40 GHz) with typical turnaround times of 10 h (for simulating 25 ms at 1000 Hz; using two cores) to 48 h (for 3 ms at 8000 Hz; using four cores).

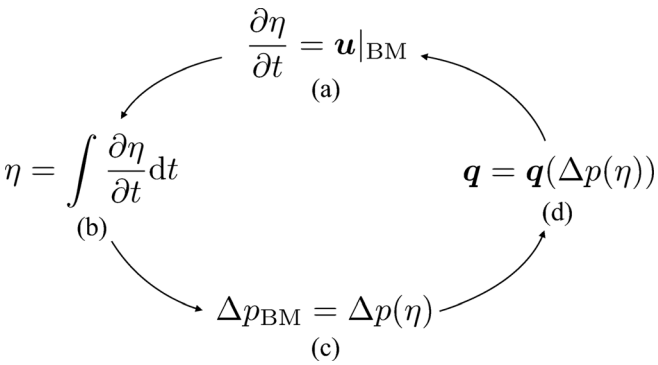


FIG. 2. Mobility formulation of the fluid-structure interaction: (a) The membrane velocity is induced by the local flow velocities, (b) integration in time of the membrane velocity yields the displacements, (c) the displacement leads to a pressure difference across the BM, Eq. (5), (d) the pressure difference affects the fluid as a field force, Eq. (2).

## III. RESULTS

The simulations are carried out at Reynolds numbers of $\mathrm{Re} = 0.09$–$0.9$ ($\nu^* = 1 \times 10^{-6}$ m$^2$/s, $L^* = 3 \times 10^{-3}$ m, different maximum stapes velocities $U^*$). We simulate first with constant velocity amplitude for all frequencies for RSM and PSM. Second, we impose stapes velocities which were measured by Sim *et al.* (2010) at constant ear canal sound pressure level. This results in different velocities with respect to stapes frequency and movement type. Figure 3 indicates the stapes velocities at 1 Pa ear canal pressure amplitude, equivalent to 94 dB sound pressure level. For the constant-amplitude simulations we use a maximum stapes velocity of $U^* = 3 \times 10^{-5}$ m/s.

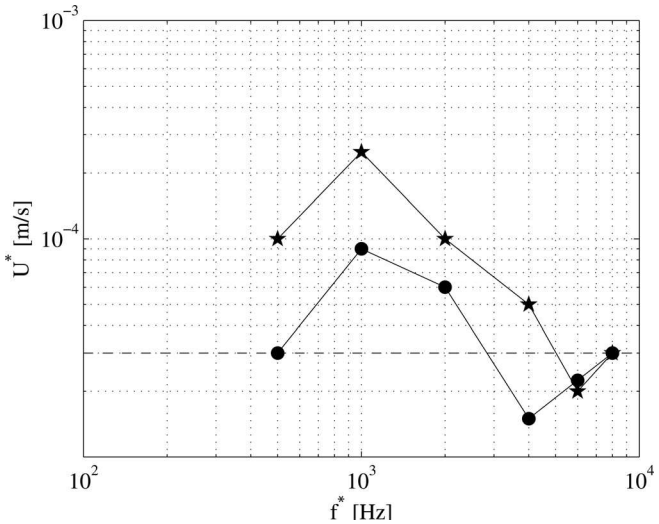


FIG. 3. Stapes velocities $U^*$ for different frequencies [⋆: PSM, ●: RSM, both from Sim *et al.* (2010) at 1 Pa ear canal pressure amplitude, - - -: value for constant-velocity simulations].

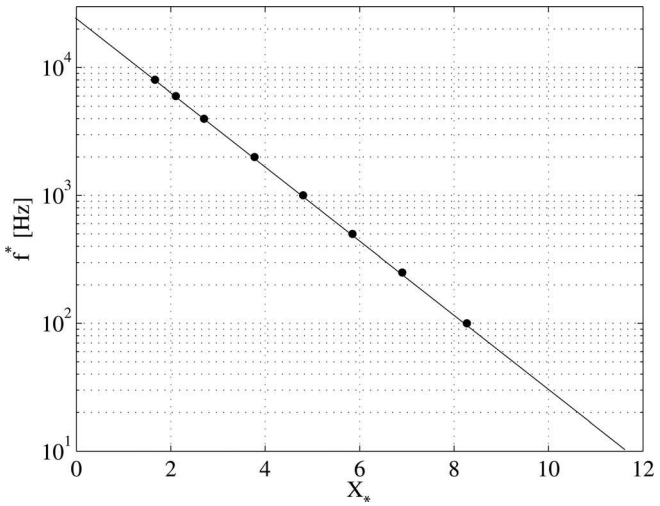


FIG. 4. Tonotopic map of the cochlea model (●: computed characteristic place, ——: approximated exponential scaling).

The BM stiffness decays exponentially along the cochlear length and is scaled such that frequencies from roughly 20 Hz to 20 kHz are mapped exponentially along the membrane as shown in Fig. 4. The stiffness at the base of the membrane is $k^*_{\text{base}} = 6.25 \times 10^{11}\,\text{N/m}^3$ and decays exponentially to $k^*_{\text{apex}} = 6.25 \times 10^5\,\text{N/m}^3$ at the apex. These values were chosen *ad hoc* to obtain a reasonable tonotopic map.

### A. General aspects of the fluid motion

The flow fields for the stapes modes RSM and PSM differ significantly in the region close to the stapes. Figure 5 shows respective flow fields in the basal region. The flow field for the RSM [Fig. 5(a)] is taken at the time point when the right edge of the stapes moves into the cochlea. This leads to a fluid motion in the clockwise direction beneath the OW, while there is no flow at the RW. Figure 5(b) shows the flow field for the PSM when the stapes is moving out of the cochlea. This creates a net outflow at the OW and a corresponding net inflow at the RW.

Further into the cochlea (Fig. 6) the flow field for the RSM features a traveling wave which looks nearly the same as the traveling wave for a PSM (not shown here). However, the velocity amplitudes in the traveling wave due to the RSM are generally much smaller than the amplitudes generated by a PSM of comparable intensity. In addition to the classical velocity maximum at the characteristic place, traveling wave flow fields due to a RSM also have local velocity maxima beneath the stapes which are typically of lesser amplitude.

### B. Traveling wave motion of the BM

Figure 7 shows the displacement of the BM for PSM and RSM (the amplitude is normalized, values are discussed in Sec. III C). Both the PSM and RSM produce a traveling wave on the BM. The shape of both waves is identical, except for small deviations in the region below the stapes ($X < 1$). No phase shift between the traveling waves is observed if the PSM is in phase with the left edge of the RSM [as it is shown in Figs. 5 and 11(a)]. In accordance with these findings, the normalized envelopes of the traveling waves show differences only in the basal region below the stapes.

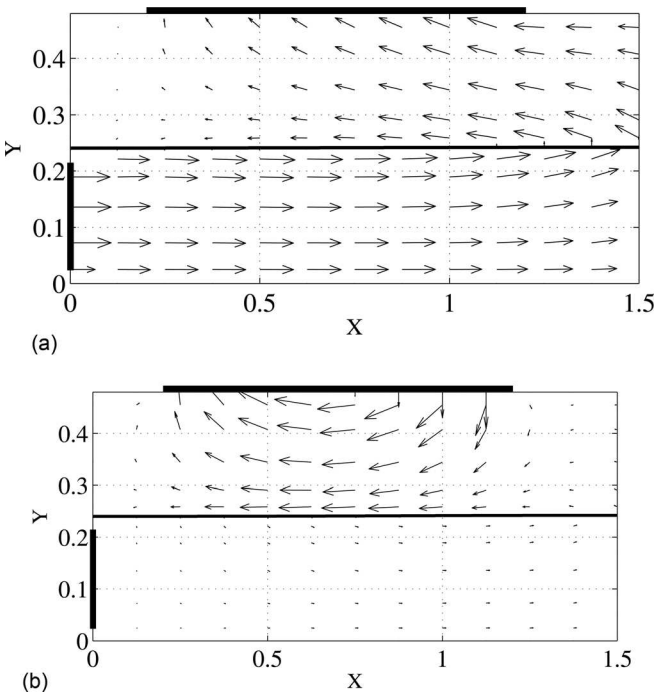


FIG. 5. Velocity vectors in the basal region for a stimulation at $f^* = 1000$ Hz with (a) RSM and (b) PSM. The flow fields are shown at the time point when the stapes (indicated by a bold line) is moving (a) with its right edge into the cochlea and (b) out of the cochlea at maximum velocity (——: BM, bold lines: OW and RW).

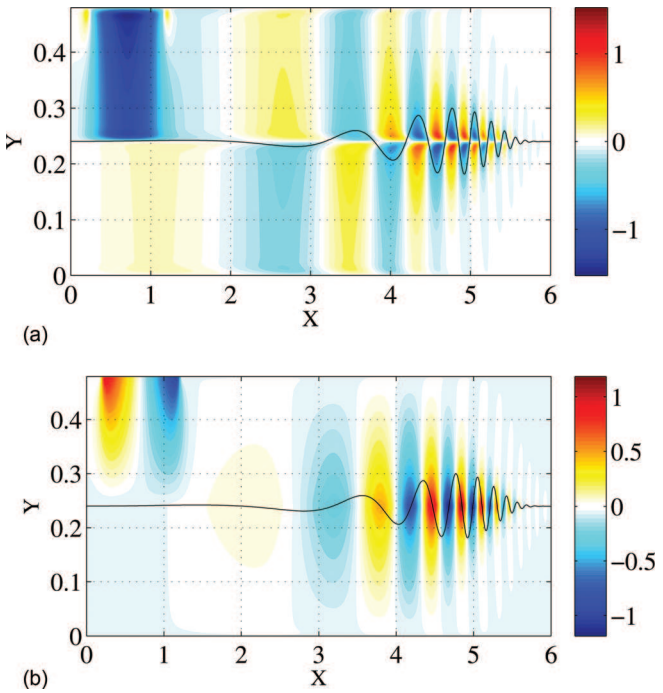


FIG. 6. Velocity components of the instantaneous flow field for RSM in the basal half of the computational domain; $f^* = 1000$ Hz, steady state. The stapes is at its instantaneous maximum velocity of $u_{\text{in}} = 1$ with the right edge moving into the cochlea (——: exaggerated BM displacement).

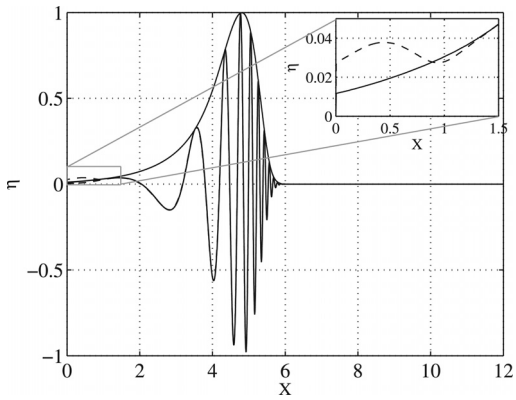


FIG. 7. Envelope and instantaneous displacement of the BM for PSM and RSM at 1000 Hz with normalized amplitude (——: PSM, - - - RSM). Inset shows only the envelopes.

### C. Peak amplitudes for rocking and piston-like stapes motion

Figure 8 shows envelopes of the computed BM displacement as a function of location for different frequencies [for PSM in Fig. 8(a) and for RSM in Fig. 8(b)]. In these numerical experiments, the maximum stapes velocity is $U^* = 3 \times 10^{-5}$ m/s for both modes and for all stimulation frequencies. For the PSM, we find the well-known result that the maximum BM amplitude at the characteristic place decreases as the stimulation frequency increases. For the RSM, the peak amplitude increases as the frequency increases. This behavior persists up to $f^* \approx 2000$ Hz. For higher frequencies, the peak amplitudes due to RSM decrease steeply. In these cases, i.e., when the characteristic place is close to the stapes, the traveling wave on the BM seems to interact directly with the flow field close to the stapes [see Fig. 5(a)]. Given the simplified geometry in the basal region of our box model (Fig. 1), the amplitudes for the high frequencies might not be directly applicable to the anatomical conditions.

In Fig. 9, the results of Fig. 8 are summarized. It shows the maximum BM amplitudes for PSM and RSM as a function of the stimulation frequency. For a given frequency, we find that the peak amplitude for RSM is always smaller than the one for PSM. The difference between the peak amplitudes is smallest at around 4000 Hz where the RSM amplitude is approximately 10 dB smaller than the PSM amplitude. If we assume that the stapes velocity scales linearly with the sound pressure level, we can interpret this difference as an indication on how much softer a tone would be perceived if there was no piston-like component of the stapes motion. For stimulation frequencies below 4000 Hz, the difference between the peak amplitudes for RSM and PSM increases by about 12 dB per octave and it reaches about 70 dB at 100 Hz. (Figure 9 will be further discussed in Secs. III E and III F.)

All data points in Fig. 9 were obtained for the same maximum stapes velocity. In contrast to this, Fig. 10 shows the peak BM amplitudes obtained for actual stapes velocities measured by Sim *et al.* (2010) for a sound pressure level of 94 dB in the ear canal. The significant differences between the RSM and PSM stapes velocities (see Fig. 3) further increase the differences between the respective peak BM amplitudes. The smallest peak difference of approximately

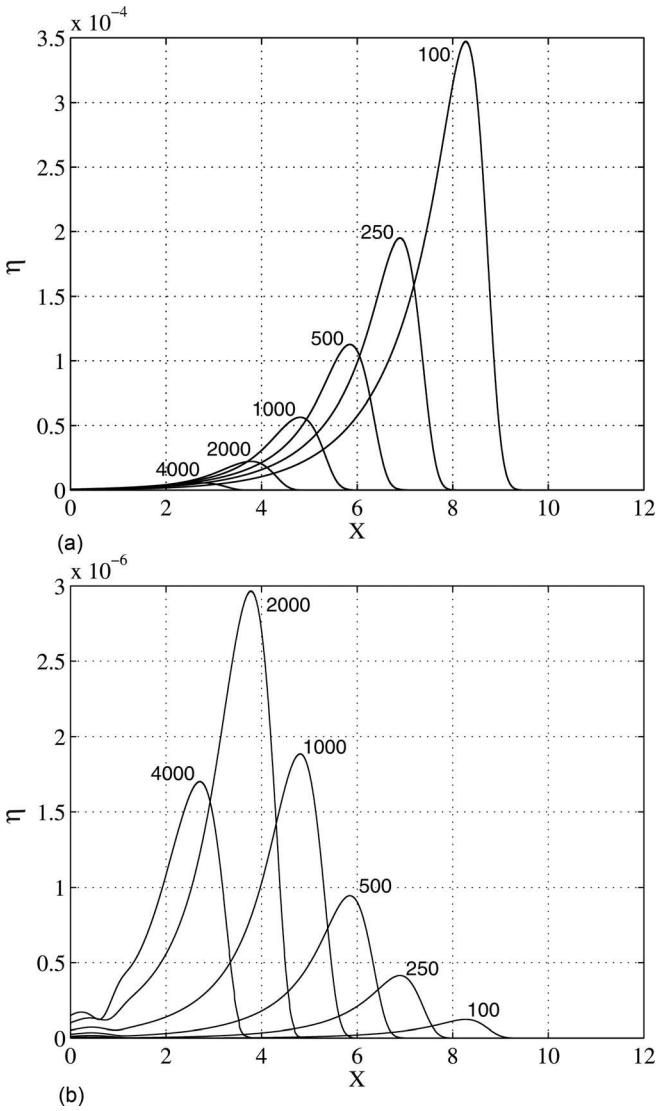


FIG. 8. Envelopes of the BM oscillation for PSM and RSM at different frequencies given in Hz with the same maximum stapes velocity of $3 \times 10^{-5}$ m/s for all simulations.

20 dB is now found in the frequency range between 2000 and 4000 Hz.

### D. Combined stapes motion

The combination of PSM and RSM either increases or decreases the amplitudes which are generated by PSM alone, depending on the phase shift between the two modes. Neither the shape of the traveling wave nor its envelope changes qualitatively. The maximum increase is reached if the traveling waves of both stapes displacements are in phase, which is the case if the PSM is in phase with the left stapes edge for the RSM (case AA in Fig. 11). The minimum amplitudes occur if the PSM is in phase with the right edge (case AB in Fig. 11). In this case, the traveling waves generated by both stapes displacements interfere destructively. Figure 11 shows the envelopes for simulations with combined stapes motion and with pure PSM or RSM. For the combined stimulations, the phase shifts between both components are chosen as described above and the maximum inflow velocities are $u_{in} = 1$ for both stimulation modes.

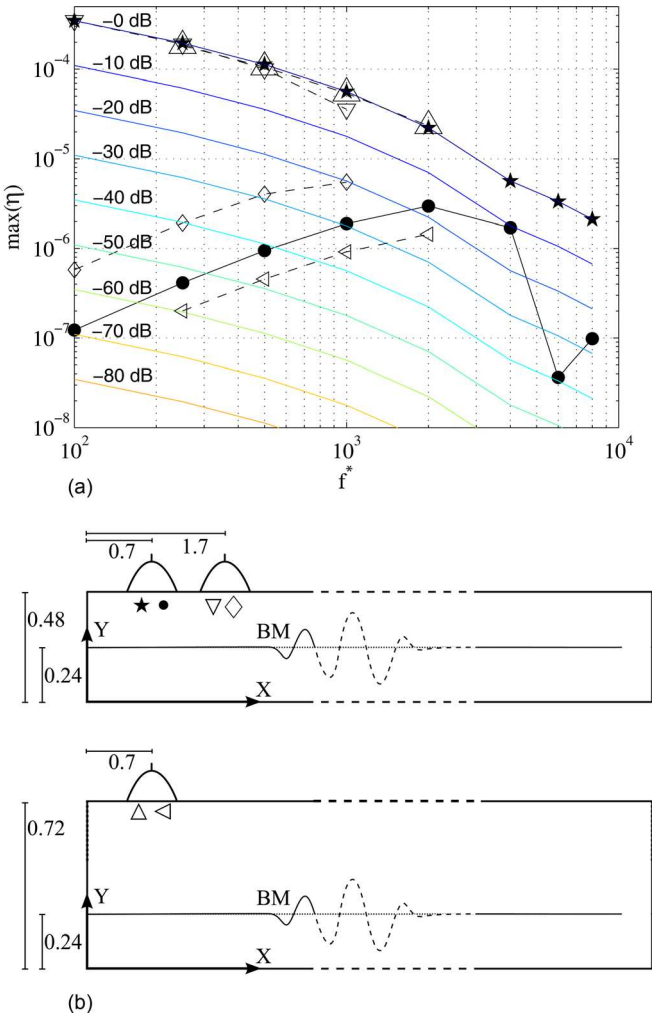


FIG. 9. (Color online) (a) Maximum BM amplitudes as a function of the stimulation frequency for RSM and for PSM and for different positions of the stapes. The maximum stapes velocity is $U^* = 3 \times 10^{-5}$ m/s for all simulations. The symbols ⋆ (PSM) and ● (RSM) indicate results for the stapes footplate centered at $X_s = 0.7$, $Y_s = 0.48$ (standard configuration, cf. Fig. 1); for ▽ (PSM) and ◇ (RSM) the stapes is centered at $X_s = 1.7$, $Y_s = 0.48$ (Sec. III E); for △ (PSM) and ◁ (RSM) the height of the scala vestibuli is doubled such that the stapes is centered at $X_s = 0.7$, $Y_s = 0.72$ (Sec. III F). The different symbols used in (a) are explained graphically in (b) which indicates the stapes position for the different test cases.

The computed envelopes for the combined stimulation shown in Fig. 11 could also be obtained by a linear superposition of the two envelopes for the pure PSM and RSM.

Accordingly, the peak amplitude difference between the combined and the purely PSM is of the same order of magnitude as the peak amplitude generated by RSM.

### E. Influence of the longitudinal stapes position

If the stapes position is somewhat shifted in the longitudinal direction, the peak amplitudes of both stimulation modi are affected. Figure 9 shows the amplitudes for the stapes footplate center situated at $X_s = 1.7$ as well as the amplitudes for the stapes centered at $X_s = 0.7$. The membrane displacements decrease slightly for the PSM and increase more for the RSM. The difference between the two stimulations therefore decreases by more than 10 dB.

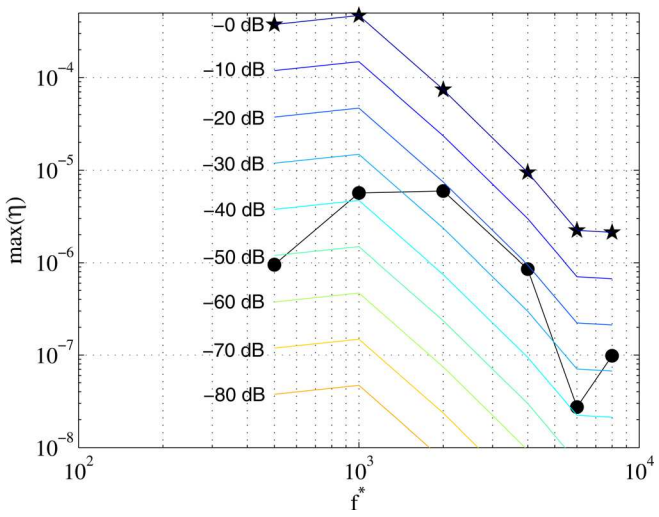


FIG. 10. (Color online) Maximum BM amplitudes as a function of the stimulation frequency for PSM (⋆) and RSM (●). The respective stapes velocities are taken from measurements by Sim *et al.* (2010) which were obtained for an acoustic stimulation with 94 dB in the ear canal. The stapes footplate is centered at $X_s = 0.7$, $Y_s = 0.48$.

### F. Influence of the distance between stapes and BM

Figure 9 also indicates the peak amplitudes for the two stimulation modes if the distance between the stapes and the BM is doubled ($Y_s = 0.72$, $Y_{BM} = 0.24$) by doubling the height of the SV. The PSM amplitudes are practically not affected by the change, whereas the RSM amplitudes show an additional loss of 6 dB. This loss is constant for all frequencies.

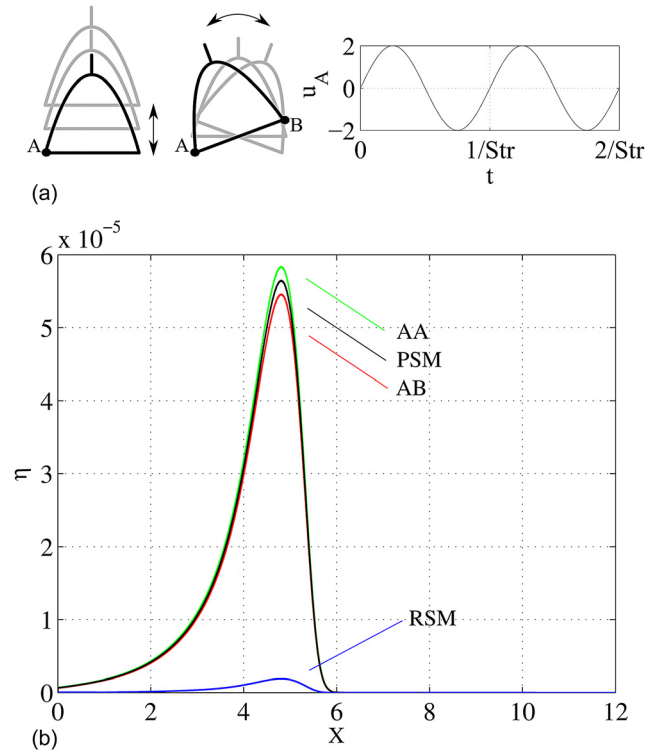


FIG. 11. (Color online) (a) Velocity of point *A* for combined stapes motion if point *A* of PSM is in phase with point *A* of RSM (case AA). (b) Envelopes for stimulation with pure PSM or RSM and with combinations of both at $f^* = 1000$ Hz. Simulation with maximum inflow velocity $u_{in} = 1$ for both components [AA: point *A* of PSM in phase with point *A* of RSM, AB: point *A* of PSM in phase with point *B* of RSM, see panel (a)].

## IV. DISCUSSION

### A. Different modes of membrane excitation

The results in Sec. III C showed that the peak amplitudes of the BM increase with decreasing frequency for the PSM whereas they decrease for the RSM below 2000 Hz. In Sec. III E we have seen that a change in the longitudinal position of the stapes influences the amplitude for the RSM considerably whereas the amplitudes for the PSM are barely changed. Finally, we have seen in Sec. III F that the distance between the stapes and the BM affects the RSM amplitudes but not the amplitudes generated by PSM. These observations can be explained on the basis of potential flow theory and by different mechanisms which excite the BM motion.

#### 1. Potential flow in the cochlea

The fluid flow in the cochlea can be approximated as potential flow since the bulk of the flow field is irrotational and the boundary layers are thin (Lesser and Berkley, 1972). Therefore, the velocity field $\boldsymbol{u}$ can be described by a potential $\Phi$ with

$$\boldsymbol{u} = \nabla\Phi. \tag{6}$$

The pressure field can be derived from the unsteady Bernoulli equation which reads

$$\mathrm{Str}\frac{\partial\Phi}{\partial t} + \frac{1}{2}|\nabla\Phi|^2 + p = 0 \tag{7}$$

in dimensionless form. For an oscillating flow field the first term $\partial\Phi/\partial t$ scales with the Strouhal number (3). Within the bulk region of the flow, the second term $|\nabla\Phi|^2$ remains of order 1. For high frequencies, we can approximate the pressure $\hat{p}$ to first order by neglecting the nonlinear term (using complex number notation with $i^2 = -1$)

$$\hat{p} = i\,\mathrm{Str}\,\hat{\Phi}, \tag{8}$$

where

$$(p, \Phi) = (\hat{p}, \hat{\Phi})\exp it. \tag{9}$$

Expression (8) shows that the amplitude of the pressure oscillation depends linearly on the stimulation frequency whereas the potential $\Phi$ and the velocity field $\boldsymbol{u}$ remain independent of the frequency.

In the framework of the potential flow theory, the cochlear fluid motion induced by the PSM can be modeled as the flow generated by a source and a sink at the positions of the oval and round windows, respectively, and the RSM can be modeled as a dipole (Pozrikidis, 2008).

The dipole potential which models RSM is given by

$$\Phi_{\mathrm{dipole}} = \mu\frac{x}{x^2 + y^2} \tag{10}$$

with the dipole intensity $\mu$. The origin of the coordinates $(x, y)$ is at the stapes and $x$ points toward the apex. The dipole potential (10) neglects the presence of the cochlear walls and of the flexible BM, but it is sufficient for showing that the pressure amplitude in the slender scala vestibuli decays like $1/x$ while the velocity decays more rapidly like $1/x^2$.

It follows from Eqs. (8) and (10) that for RSM the pressure along the BM is

$$\hat{p}_{\mathrm{BM}}(X) = i\,\mathrm{Str}\,\mu\frac{X - X_s}{(X - X_s)^2 + H^2}, \tag{11}$$

where $X_s$ is the longitudinal position of the stapes footplate center and $H$ is the height of the scala vestibuli (cf. Fig. 1). Because the RSM pressure in the scala tympani is very small (i.e., nearly equal to the middle ear pressure), the pressure $\hat{p}_{\mathrm{BM}}$ is an approximation for the pressure difference $\Delta p$ across the BM. From Eq. (11) we then find that the spatial maximum of the pressure difference across the BM scales like

$$\max_X \hat{p}_{\mathrm{BM}} \propto \mathrm{Str}/H. \tag{12}$$

#### 2. Amplitude scaling and modes of membrane excitation

We can now use these results from the potential flow theory to explain the amplitude scaling for RSM as it is illustrated in Fig. 9. To this end, we hypothesize that the RSM can initiate the traveling wave only beneath the stapes at $X \approx X_s$, because the pressure difference across the BM decays so rapidly away from the stapes. In the model presented in this work, the BM amplitude $\hat{\eta}$ depends on the inverse membrane stiffness and on the force acting on the membrane which scales with the pressure difference across the BM. Therefore, we postulate that the BM peak amplitudes for RSM scale as

$$\hat{\eta} \propto \frac{\mathrm{Str}}{Hk(X_s)}, \tag{13}$$

where $k(X_s)$ is the BM stiffness beneath the stapes.

Figure 12 shows peak BM amplitudes obtained from our cochlear model (same data as in Fig. 9) compared to the predictions obtained from Eq. (13). A comparison of these data sets shows that the increase of the BM amplitude due to a longitudinal shift of the stapes is well predicted by Eq. (13). In contrast to the RSM-evoked amplitudes, the amplitudes due to PSM (Fig. 9) are nearly independent of the longitudinal stapes position (for sufficiently small frequencies). Apparently, the flow and pressure field in the vicinity of the characteristic place is almost unaffected by the stapes position for PSM. This observation is directly related to the oscillating fluid column between the stapes and the characteristic place. The fluid velocity in this column depends on the net fluid displacement due to PSM but is independent of the stapes location, such that the BM amplitude is also independent of $X_s$.

Furthermore, Fig. 12 shows BM amplitudes due to RSM in a cochlea with a doubled height for the scala vestibuli. Therefore, the distance between the stapes footplate and the BM is increased to $2H$. We observe in Fig. 12 that the BM amplitude is reduced by a factor of 2 which again agrees well with Eq. (13).

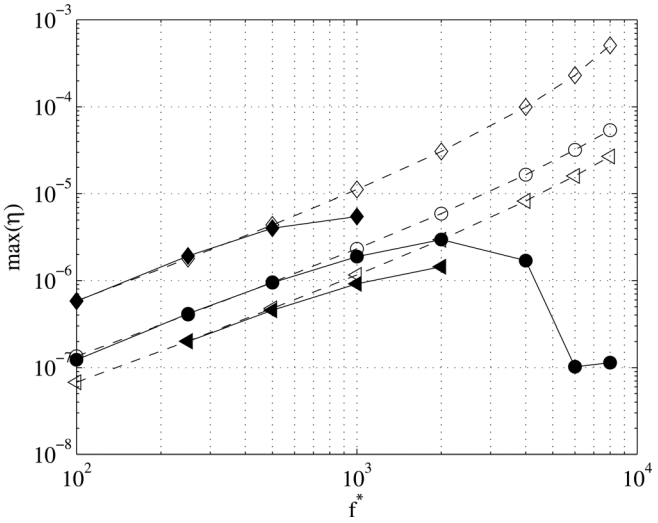


FIG. 12. Scaling of the peak amplitudes due to RSM with the same maximum stapes velocity for all data points [——: simulated, - - -: scaling for RSM, $\hat{\eta} \propto \mathrm{Str}/(Hk(X_s))$, for different stapes positions: ◆,◇: stapes footplate center at $X_S = 1.7$, $Y_S = 0.48$; ●,○: stapes footplate center at $X_S = 0.7$, $Y_S = 0.48$; ◀, ◁: stapes footplate center at $X_S = 0.7$, $Y_S = 0.72$].

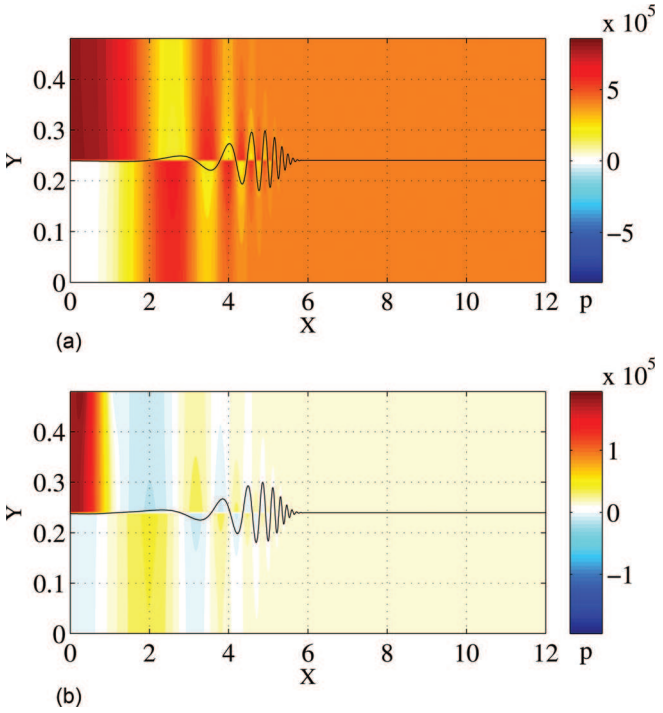


FIG. 13. Pressure fields for PSM and RSM stimulation taken at the time of maximum pressure in the cochlea; $p = 0$ at the RW, $f^* = 1000$ Hz. For the PSM, the stapes has reached the maximum velocity $u_{\mathrm{in}} = 1$, moving into the cochlea; for the RSM, the left stapes edge has reached the maximum deflection out of the cochlea and starts moving into the cochlea, $u_{\mathrm{in}} = 0$ (——: BM displacement, exaggerated).

As the characteristic place approaches the stapes, increasing differences between the scaling (13) and the simulated results can be seen in Fig. 12 (for $f^* \gtrsim 1000$ Hz). As stated in Sec. III C, these differences arise due to direct interactions between the inflow at the stapes and the traveling wave on the BM. This is supported by the fact that the deviations begin at lower frequencies for the shifted stapes position ($X_s = 1.7$).

Figure 13 shows instantaneous pressure fields for both stimulation modes. In contrast to the simplified potential flow model, this result has been obtained with the full model and includes also effects from the walls, the fluid viscosity and the flexible BM. The no-slip boundary conditions at the walls and BM lead to narrow viscous boundary layers which introduce damping to the system. (Without fluid viscosity, this damping would have to be modeled through the BM damping $r$.) The pressure wave due to PSM reaches the characteristic place with significantly larger relative amplitudes than for the RSM, whereas the RSM pressure field features relatively large pressures beneath the stapes but only a weak pressure wave. The instants of maximum pressure amplitudes shown in this figure occur at different phases: for the PSM when the maximum stapes velocity is reached, and for the RSM at zero stapes velocity.

Figure 14 shows the amplitudes of the pressure differences $\Delta p_{\mathrm{BM}}$ across the BM for RSM and for PSM. We find that the pressure difference due to RSM beneath the stapes ($X \lessapprox 1$) decays rapidly in the longitudinal direction which is in accordance with potential flow theory (11). For $X \gtrapprox 1$, the traveling wave dominates the pressure field such that the curve for RSM corresponds to the PSM curve with an amplitude shift.

### B. Box geometry in the high-frequency region

In most existing box models of the cochlea, the oval and round windows are located at the front side ($X = 0$) of the box, positioned orthogonal to the BM. The resulting symmetry allows considering only either of the SV or ST, leading to a less expensive model setup. However, investigations with human temporal bones (e.g., Eaton-Peabody Laboratory of Auditory Research, 2009) showed that the OW is situated at the side wall of the SV rather than at its front side. Therefore, we locate the stapes on the upper side of the cochlear wall (Fig. 1).

The best estimate of the RW location is not obvious since the hook region of the cochlea is anatomically complicated. As the cochlear duct terminates at the posterior edge of the RW (Nager, 1993; Stidham and Roberson, 1999;

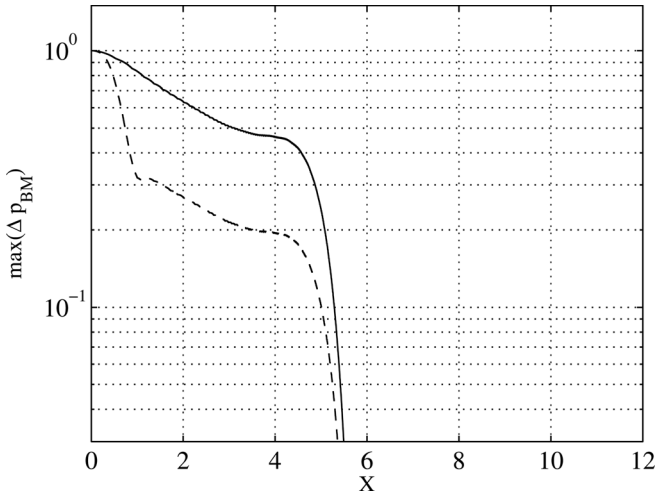


FIG. 14. Normalized envelopes of the vertical pressure difference across the BM, $f^* = 1000$ Hz (——: PSM, - - -: RSM).

Li *et al.*, 2007), we position the RW at the front side of the ST. On the other hand, the RW is mostly parallel to the BM such that its location on the side wall of the ST is possible as well (Steele *et al.*, 2008).

### C. Significance of the rocking stapes motion for the perception of sound

In a clinical context, a situation similar to the presented model with RSM can be found in patients with round window atresia. In this condition, the RW is not covered by a deformable membrane but by solid bone. Therefore no net volume displacement can be generated at the stapes. Linder *et al.* (2003) presented the hearing ability of patients suffering from round window atresia. Instead of a total conductive hearing loss, they observed mixed hearing losses with air-bone gaps of 15–30 dB. (The air-bone gap is the threshold difference between the sound perception by air and by bone conduction and is a measure for the loss of air-conductive sound transmission.) This finding is an indication of cochlea activation through rotational stapes motions since the observed hearing ability cannot be explained if net fluid shifts due to PSM are assumed to be the only effective stimulus of the cochlea. Alternative explanations to these findings are cochlear receptors that are sensitive to intracochlear pressure or a nonzero compressibility of the cochlea. This may be related to fluid flow out of the cochlea through the perilymphatic or endolymphatic ducts (third window effect) or compressibility of tissue. Although such effects have been proven to be small in normal ears (Shera and Zweig, 1992; Voss *et al.*, 1996) they might become dominant in pathological situations.

Clinical situations similar to the presented model can be found also in patients with middle ear prostheses. Beltrame *et al.* (2009) study the hearing ability of patients with active middle ear prostheses on the RW which have been implanted because of conductive or mixed hearing loss. These studies comprise patients with fixed stapes, i.e., cases in which no net volume displacement is possible if the stimulation takes place at the RW. Hearing recovery is reported also from these patients, even if with smaller functional gain than in other patients, which indicates that the cochlea can be activated without net volume displacement at the OW or the RW.

## V. CONCLUSIONS

Both the piston-like (PSM) and the rocking component (RSM) of the stapes movement generate a traveling wave in the fluid and on the BM. The fluid motion shows qualitative differences only in the basal region. Likewise, the normalized traveling waves of the BM evoked by the two stimulations are identical except at the basal end.

The PSM evokes higher amplitudes than the RSM, a difference which increases with decreasing frequency. At identical stapes velocity amplitudes, the minimum difference in the peak amplitude of the BM is found at 4000 Hz. Here, the amplitude for the RSM corresponds to a PSM-evoked tone if that one is stimulated softer by 10 dB. Toward lower frequencies, the difference increases by about 12 dB per octave (Fig. 9). At identical sound pressure levels where the stapes velocity is lower for the rotational component than for the translational one, the minimum difference (at 4000 Hz) amounts to 20 dB and increases less regularly (Fig. 10). If the stapes position is moved toward the apex, the peak BM amplitudes due to the RSM increase clearly whereas those due to the PSM remain nearly unchanged. The amplitude scaling behavior along the cochlea can be explained on the basis of potential flow theory and by the fact that the membrane motion under RSM is provoked differently than under PSM. In the case of the piston-like stimulation, the fluid motion excites the BM along its complete length. The peak amplitudes increase for lower frequencies, because softer membrane sections are activated. For RSM, the BM oscillates due to a local activation directly below the stapes.

Activation of the BM with combined stapes motion does not alter the traveling wave of the membrane. Superposition of the traveling waves resulting from the single-mode stimulation yields the same BM motion as simulations with combined stimulation. The maximum amplitude difference equals the peak amplitude generated by the RSM.

Under normal conditions, when the cochlea is activated by both stapes movements at the same time, the traveling wave on the membrane is dominated by the PSM component and the RSM has almost no influence on the amplitudes. Under pathological conditions the PSM might be prevented, e.g., by round window atresia. In this situation, the RSM leads to the perception of tones. The hearing loss then amounts to about 20 dB for higher frequencies ($f^* \gtrsim 2000$ Hz) and increases for lower ones.

## ACKNOWLEDGMENTS

This work was supported by ETH Research Grant No. ETH-1709-2 (E.E.) and by SNF Project No. 31000-120237 (J.H.S., A.M.H.).

Békésy, G. (**1960**). *Experiments in Hearing* (McGraw-Hill, New York), pp. 95–126.

Beltrame, A. M., Martini, A., Prosser, S., Giarbini, N., and Streitberger, C. (**2009**). "Coupling the vibrant soundbridge to cochlea round window: Auditory results in patients with mixed hearing loss," Otol. Neurotol. **30**, 194–201.

Beyer, R. (**1992**). "A computational model of the cochlea using the immersed boundary method," J. Comput. Phys. **98**, 145–162.

Decraemer, W. F., de la Rochefoucauld, O., Dong, W., Khanna, S. M., Dirckx, J. J. J., and Olson, E. S. (**2007**). "Scala vestibuli pressure and three-dimensional stapes velocity measured in direct succession in gerbil," J. Acoust. Soc. Am. **121**, 2774–2791.

de la Rochefoucauld, O., and Olson, E. S. (**2007**). "The role of organ of Corti mass in passive cochlear tuning," Biophys. J. **93**, 3434–3450.

Drazin, P., and Riley, N. (**2006**). *The Navier Stokes Equations A Classification of Flows and Exact Solutions, Vol. 334 of London Mathematical Society Lecture Note Series* (Cambridge University Press, New York), p. 6.

Eaton-Peabody Laboratory of Auditory Research, Boston (2009). http://research. meei.harvard.edu/otopathology/3dmodels (Last accessed November 25, 2012).

Eiber, A., Huber, A. M., Lauxmann, M., Chatzimichalis, M., and Sim, J. H. (**2012**). "Contribution of complex stapes motion to cochlea activation," Hear. Res. **284**, 82–92.

Ferziger, J. H., and Perić, M. (**2002**). *Computational Methods for Fluid Dynamics*, 3rd ed. (Springer-Verlag, Berlin), pp. 188–202.

Givelberg, E., and Bunn, J. (**2003**). "A comprehensive three-dimensional model of the cochlea," J. Comput. Phys. **191**, 377–391.

Hato, N., Stenfelt, S., and Goode, R. L. (**2003**). "Three-dimensional stapes footplate motion in human temporal bones," Audiol. Neuro-Otol. **8**, 140–152.
Henniger, R., Obrist, D., and Kleiser, L. (**2010**). "High-order accurate solution of the incompressible Navier-Stokes equations on massively parallel computers," J. Comput. Phys. **229**, 3543–3572.
Huber, A. M., Sequeria, D., Breuninger, C., and Eiber, A. (**2008**). "The effects of complex stapes motion on the response of the cochlea," Otol. Neurotol. **29**, 1187–1192.
Lesser, M. B., and Berkley, D. A. (**1972**). "Fluid mechanics of the cochlea. Part 1," J. Fluid Mech. **51**, 497–512.
Li, P. M. M. C., Wang, H., Northrop, C., Merchant, S. N., and Nadol, J. B. (**2007**). "Anatomy of the round window and hook region of the cochlea with implications for cochlear implantation and other endocochlear surgical procedures," Otol. Neurotol. **28**, 641–648.
Lighthill, J. (**1981**). "Energy flow in the cochlea," J. Fluid Mech. **106**, 149–213.
Lighthill, J. (**1992**). "Acoustic streaming in the ear itself," J. Fluid Mech. **239**, 551–606.
Linder, T. E., Ma, F., and Huber, A. (**2003**). "Round window atresia and its effects on sound transmission," Otol. Neurotol. **24**, 259–263.
Nager, G. T. (**1993**). *Pathology of the Ear and Temporal Bone* (Williams & Wilkins, Baltimore), pp. 3–7.
Peskin, C. S. (**2002**). "The immersed boundary method," Acta Numerica **11**, 479–517.
Peterson, L. C., and Bogert, B. P. (**1950**). "A dynamical theory of the cochlea," J. Acoust. Soc. Am. **22**, 369–381.
Pozrikidis, C. (**2008**). "Boundary-integral modeling of cochlear hydrodynamics," J. Fluids Struct. **24**, 336–365.
Shera, C. A., and Zweig, G. (**1992**). "An empirical bound on the compressibility of the cochlea," J. Acoust. Soc. Am. **92**, 1382–1388.
Sim, J. H., Chatzimichalis, M., Lauxmann, M., Röösli, C., Eiber, A., and Huber, A. M. (**2010**). "Complex stapes motions in human ears," J. Assoc. Res. Otol. **11**, 329–341.
Steele, C. R., Baker, G. J., Tolomeo, J. A., and Zetes-Tolomeo, D. E. (**1995**). *The Biomedical Engineering Handbook* (CRC Press, Boca Raton, FL), Chap. 63, p. 63-3.
Steele, C. R., Kim, N. K., and Puria, S. (**2008**). "Hook region represented in a cochlear model," in *Concepts and Challenges in the Biophysics of Hearing: Proceedings of the 10th International Workshop on the Mechanics of Hearing*, pp. 323–329.
Stidham, K. R., and Roberson, J. B. (**1999**). "Cochlear hook anatomy: Evaluation of the spatial relationship of the basal cochlear duct to middle ear landmarks," Acta Otolaryngol. **19**, 773–777.
Stuhlman, O., Jr. (**1937**). "The nonlinear transmission characteristics of the auditory ossicles," J. Acoust. Soc. Am. **9**, 119–128.
Voss, S. E., Rosowski, J. J., and Peake, W. T. (**1996**). "Is the pressure difference between the oval and round windows the effective acoustic stimulus for the cochlea?," J. Acoust. Soc. Am. **100**, 1602–1616.